Electrostatic Interactions Affect Nanoparticle-Mediated Toxicity to Gram-Negative Bacterium *Pseudomonas aeruginosa* PAO1

Kevin Feris,[†] Caitlin Otto,[†] Juliette Tinker,[†] Denise Wingett,[†] Alex Punnoose,[‡] Aaron Thurber,[‡] Madhu Kongara,[‡] Maryam Sabetian,[‡] Bonnie Quinn,[§,||] Charles Hanna,[‡,||] and David Pink*[,§,||]

[†]*Department of Biology, and* [‡]*Department of Physics, Boise State University, Boise, Idaho 83725,* [§]*Department of Physics, St. Francis Xavier University, Antigonish, Nova Scotia, Canada B2G2W5, and* [||]*Advanced Foods and Materials Network Canada*

Nanoscale materials can have cytotoxic effects. Here we present the first combined empirical and theoretical investigation of the influence of electrostatic attraction on nanoparticle cytotoxicity. Modeling electrostatic interactions between cells and 13 nm spheres of zinc oxide nanoparticles provided insight into empirically determined variations of the minimum inhibitory concentrations between four differently charged isogenic strains of *Pseudomonas aeruginosa* PAO1. We conclude that controlling the electrostatic attraction between nanoparticles and their cellular targets may permit the modulation of nanoparticle cytotoxicity.

1. Introduction

Nanoparticles (NPs), natural and manufactured substances with sizes in the range of 1−100 nm, have been proven to be valuable materials for sensing and manipulating biological systems. However, many of these materials demonstrate cytotoxic properties in a wide range of eukaryotic and prokaryotic cells.[1−8] One of the recognized mechanisms of metal oxide NP-induced toxicity (e.g., ZnO, TiO_2, etc.) has been attributed to the formation of reactive oxygen species (ROS) upon NP exposure.[9−12] Conduction electrons (freely moving electrons in the conduction band) and valence holes (the absence of valence electrons or vacancies in the valence band) in semiconductors such as ZnO and TiO_2 have been traditionally used for the photocatalytic oxidation of organic and inorganic pollutants and sensitizers for the photodestruction of cancer cells,[13−15] bacteria,[16,17] and viruses[18] via oxidative damage.[19] Although in these experiments adequate electrons and holes are usually produced via UV irradiation and excitation, in NPs, large numbers of holes and/or electrons might be available even without the presence of UV light. The holes are powerful oxidants and can react with water or surface-bound chemisorbed hydroxyl groups to produce hydroxyl radicals. The conduction band electrons are good reductants and can move to the particle surface and get trapped in metastable surface states or react with electron acceptors or oxidants such as adsorbed O_2. The band gap, which influences the difference between the energies of the conduction electrons and valence holes in semiconductors such as ZnO and TiO_2, provides sufficiently large overpotentials for redox reactions and ROS production. NP-induced toxicity via ROS-mediated cellular damage has been most clearly and extensively demonstrated in eukaryotic cells.[1,4,20−25] Less is known about the mode of toxicity in bacterial cell systems, although some investigators have proposed similar ROS-dependent mechanisms.[26−28] Although these studies have illuminated certain aspects of the mechanism of NP cytotoxicity, further research is needed to describe the specific interactions between cells and NPs as a means of understanding NP cytotoxicity. We have performed what are, to the best of our knowledge,

*Corresponding author. E-mail: david pink_scorpiocarla@gmail.com.

(1) Hanley, C.; Layne, J.; Punnoose, A.; Reddy, K. M.; Coombs, I.; Coombs, A.; Feris, K.; Wingett, D. *Nanotechnology* **2008**, *19*, 295103.

(2) Reddy, K. M.; Feris, K.; Wang, C.; Punnoose, A. *Appl. Phys. Lett.* **2007**, *90*, 213902.

(3) Brunner, T. J.; Wick, P.; Manser, P.; Spohn, P.; Grass, R. N.; Limbach, L. K.; Bruinink, A.; Stark, W. J. *Environ. Sci. Technol.* **2006**, *40*, 4374–4381.

(4) Deng, X. Y.; Luan, Q. X.; Chen, W. T.; Wang, Y. L.; Wu, M. H.; Zhang, H. J.; Jiao, Z. *Nanotechnology* **2009**, *20*, 11.

(5) Gwinn, M. R.; Vallyathan, V. *Environ. Health Perspect.* **2006**, *114*, 1818–1825.

(6) Liu, Y.; He, L.; Mustapha, A.; Li, H.; Hu, Z.; M., L. *J. Appl. Microbiol.* **2009**, Apr 17 Epub ahead of print.

(7) Brayner, R.; Ferrari-Iliou, R.; Brivois, N.; Djediat, S.; Benedetti, M. F.; Fievet, F. *Nano Lett.* **2006**, *6*, 866–870.

(8) Huang, Z.; Zheng, X.; Yan, D.; Yin, G.; Liao, X.; Kang, Y.; Yao, Y.; Huang, D.; Hao, B. *Langmuir* **2008**, *24*, 4140–4144.

(9) Xia, T.; Kovochich, M.; Liong, M.; Maädler, L.; Gilbert, B.; Shi, H.; Yeh, J. I.; Zink, J. I.; Nel, A. E. *ACS Nano* **2008**, *2*, 2121–2134.

(10) Choi, O.; Hu, Z. *Environ. Sci. Technol.* **2008**, *42*, 4583–4588.

(11) Zhang, Y. G.; Ma, L. L.; Li, J. L.; Yu, Y. *Environ. Sci. Technol.* **2007**, *41*, 6264–6269.

(12) Thill, A.; Zeyons, O.; Spalla, O.; Chauvat, F.; Rose, J.; Auffan, M.; Flank, A. M. *Environ. Sci. Technol.* **2006**, *40*, 6151–6156.

(13) Kubota, Y.; Shuin, T.; Kawasaki, C.; Hosaka, M.; Kitamura, H.; Cai, R.; Sakai, H.; Hashimoto, K.; Fujishima, A. *Br. J. Cancer* **1994**, *70*, 1107.

(14) Cai, R.; Hashimoto, K.; Itoh, K.; Kubota, Y.; Fujishima, A. *Bull. Chem. Soc. Jpn.* **1991**, *64*, 1268.

(15) Cai, R.; Kubota, Y.; Shuin, T.; Sakai, H.; Hashimoto, K.; Fujishima, A. *Cancer Res.* **1992**, *52*, 2346.

(16) Matsunaga, T.; Tomoda, R.; Nakajima, T.; Wake, H. *FEMS Microbiol. Lett.* **1985**, *29*, 211.

(17) Matsunaga, T.; Tomoda, R.; Nakajima, T.; Nakamura, N.; Komine, T. *Appl. Environ. Microbiol.* **1988**, *54*, 1330.

(18) Mills, A.; Le Hunte, S. *J. Photochem. Photobiol., A* **1997**, *108*, 1–35.

(19) Imlay, J. A. *Annu. Rev. Microbiol.* **2003**, *57*, 395.

(20) Zhang, Y. B.; Chen, W.; Wang, S. P.; Liu, Y. F.; Pope, C. *J. Biomed. Nanotechnol.* **2008**, *4*, 432–438.

(21) Oberdorster, E. *Environ. Health Perspect.* **2004**, *112*, 1058–1062.

(22) Zharov, V. P.; Mercer, K. E.; Galitovskaya, E. N.; Smeltzer, M. S. *Biophys. J.* **2006**, *90*, 619–627.

(23) Choi, A. O.; Cho, S. J.; Desbarats, J.; Lovrić, J.; Maysinger, D. *J. Nanobiotechnol.* **2007**, doi:10.1186/1477-3155-5-1.

(24) Limbach, L. K.; Wick, P.; Manser, P.; Grass, R. N.; Bruinink, A.; Stark, W. J. *Environ. Sci. Technol.* **2007**, *41*, 4158–4163.

(25) Hanley, C.; Thurber, A.; Hanna, C.; Punnoose, A.; Zhang, J.; Wingett, D. *Nanoscale Res. Lett.*, in press, 2009.

(26) Adams, L. K.; Lyon, D. Y.; Alvarez, P. J. J. *Water Res.* **2006**, *40*, 3527–3532.

(27) Applerot, G.; Perkas, N.; Amirian, G.; Girshevitz, O.; Gedanken, A. *Appl. Surf. Sci.*, in press, 2009.

(28) Sawai, J.; Shoji, S.; Igarashi, H.; Hashimoto, A.; Kokugan, T.; Kojima, H. *J. Ferment. Bioeng.* **1998**, *86*, 521–522.

the first combined experiments and computer-based mathematical modeling studies to investigate whether charge-based interactions that occur prior to cellular damage are significant factors in determining whether interactions between bacterial cells and zinc oxide nanoparticles (ZnO NPs) result in cell death or survival.

Prior work has demonstrated the importance of electrostatic interactions between bacterial cell surfaces and cationic antimicrobial peptides (CAPs) in determining the efficacy of bacterial cell killing.[29,30] Pink et al.[30] employed a "minimum model" of the outer cell surface of wild-type strains of *Pseudomonas aeruginosa* and conducted Monte Carlo (MC) simulations of the interactions of the CAP protamine with the bacterial surface in the presence and absence of divalent cations. They predicted that divalent cations would replace protamine molecules in the charged region, resulting in a shift of the protamine distribution toward the aqueous solution and that, accordingly, the minimum inhibitory concentration (MIC) would increase. This prediction was confirmed by measurements, and grazing incidence X-ray scattering has since provided direct confirmation that Ca^{2+} ions partially exclude protamine.[29] There is evidence that suggests that the electrostatic properties of positively charged NPs, like CAPs, can play a role in biological membrane permeability;[31] however, less is known about these processes in the case of NPs.

We hypothesized that the bactericidal properties of metal oxide NPs are due in part to electrostatic attraction between the NP and the cell surface, affecting the time during which the NP is in the neighborhood of the cell surface, and that an increased duration of NP association with the cell surface results in increased cell killing. A minimal model was employed to provide specific predictions for how differences in the bacterial-cell surface charge would influence the energies of interaction between positively charged 13 nm ZnO NPs and the outer membrane lipopolysaccharides (LPSs) of four isogenic strains of the gram-negative bacterium *P. aeruginosa* PAO1. Implicit in this prediction is that the toxic effects of ZnO NPs are exacerbated by prolonged contact between the cell and the NP. To test the model predictions, all four strains of PAO1 were exposed to a range of ZnO NP concentrations and the effects of exposure were assessed by determining minimum inhibitory concentrations (MICs) for metabolic activity and cell viability.

The outer membrane of *P. aeruginosa* consists of a lipid bilayer with an outer leaflet of LPS (Figure 1). Under physiological conditions (pH 7.4), the sugar moieties of an LPS carry either uncharged or charged oligosaccharide chains, denoted as A and B bands, respectively. To understand the role of electrostatic interactions in determining the cytotoxicity of ZnO NPs, we employed four isogenic strains of *P. aeruginosa* PAO1. In these strains, at physiological pH, the outer leaflets consist of combinations of LPS, with the O side chains comprising uncharged trimers (A band) and charged trimers (B band), with the electric charges on the three sugars having the sequence $(0, -, -)$. Each strain possesses either a mix of charged and uncharged oligosaccharides in the LPS layer (A^+B^+ or wild type), only charged oligosaccharides (A^-B^+), only uncharged oligosaccharides (A^+B^-), or
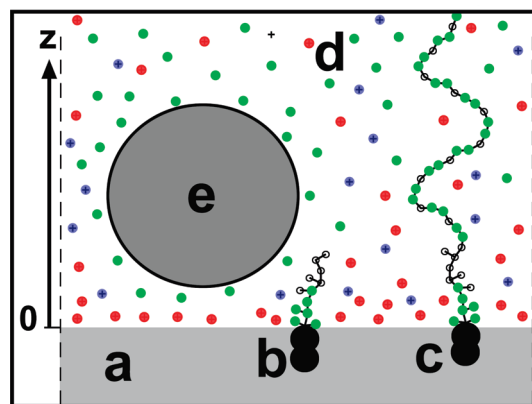

Figure 1. Schematic diagram (not to scale) of the model system. Hydrophobic layer of the outer membrane (a), with hydrocarbon chain moieties represented by large filled circles, LPS without an O side chain (b), LPS with an O side chain (c) composed of repeating trimers $(\bigcirc - \bullet - \bullet)$; ($\bullet$, green) indicating sugar groups carrying one negative charge (green) or uncharged sugar groups ($\bigcirc$). Ions in the aqueous solution (d; Na^+ blue, Cl^- green, Ca^{2+} red), and a nanoparticle (e). Here we show the B-band O side chain trimers with charge sequence $(0, -, -)$. The hydrophobic/water interface is defined as $z = 0$. The $x-y$ plane is that of the membrane.

a truncated LPS with no oligosaccharides (A^-B^-).[32,33] As described elsewhere, ~10% of the LPSs from A^-B^+, A^+B^-, or A^+B^+ strains possess O side chains[34] and were modeled as such.

Kotra et al.[35] used atomic-scale molecular dynamics to model a monolayer of 16 LPS molecules with 64 Mg^{2+} at $T = 300$ K for a total simulation time of 200 ps. Straatsma and co-workers[36,37] constructed models of outer membranes of *P. aeruginosa* consisting of 16 LPS molecules in the outer leaflet and 40 phosphatidylethanolamine molecules in the inner leaflet and ran isothermal–isobaric simulations for 1 ns to study the distribution and dynamics of Ca^{2+} and saccharide moieties. These studies demonstrated that (i) divalent cations were essential for the stability of the LPS monolayer;[35,37] (ii) most of the Ca^{2+} ions were confined to a "thin layer (20 Å) in the inner core";[36] (iii) the location of Ca^{2+} in the inner-core region was well-defined, with an average coordination number of Ca^{2+} equal to 6.1 so that the mobility of negatively charged saccharides complexed with Ca^{2+} was lower than that of uncharged saccharides;[36,37] and (iv) water penetrated the membrane to a depth of ~30 Å.[37]

2. Materials and Methods

2.1. Bacterial Strains and Cultivation Conditions. To assess the role of electrostatic interactions in controlling the cytotoxicity of ZnO NP to bacteria, four different strains of *Pseudomonas aeruginosa* PAO1 (A^+B^+, A^-B^+, A^+B^-, and A^-B^-) that differ in outer membrane characteristics were exposed to the same preparation of ZnO NP. Prior to NP exposure, PAO1 cultures were grown overnight at 37 °C with continuous shaking (200 rpm) in an LB medium. To ensure that experiments with each strain were performed with the same initial cell density, overnight cultures were adjusted to $A_{600} = 0.24$ and the viable colony-forming units per milliliter (CFU/mL) were determined by plating

(29) Oliveira, R. G.; Schneck, E.; Quinn, B. E.; Konovalov, O. V.; Brandenburg, K.; Seydel, U.; Gill, T.; Hanna, C. B.; Pink, D. A.; Tanaka, M. *C. R. Chim.* **2009**, *12*, 209–217.

(30) Pink, D. A.; Hansen, L. T.; Gill, T. A.; Quinn, B. E.; Jericho, M. H.; Beveridge, T. J. *Langmuir* **2003**, *19*, 8852–8858.

(31) Lockman, P. R.; Koziara, J. M.; Mumper, R. J.; Allen, D. D. *J. Drug Target.* **2004**, *12*, 635–641.

(32) Makin, S. A.; Beveridge, T. J. *Microbiology (Reading, U.K.)* **1996**, *142*, 299–307.

(33) Kadurugamuwa, J. L.; Lam, J. S.; Beveridge, T. J. *Antimicrob. Agents Chemother.* **1993**, *37*, 715–721.

(34) Schneck, E.; Papp-Szabo, E.; Quinn, B. E.; Konovalov, O. V.; Beveridge, T. J.; Pink, D. A.; Tanaka, M. O. *J. R. Soc. Interfaces* **2009**, *12*, doi: 10.1098/rsif.2009.0190.

(35) Kotra, L. P.; Golemi, D.; Amro, N. A.; Liu, G.-Y.; Mobashery, S. *J. Am. Chem. Soc.* **1999**, *121*, 8707–8711.

(36) Lins, R. D.; Straatsma, T. P. *Biophys. J.* **2001**, *81*, 1037–1046.

(37) Shroll, R. M.; Straatsma, T. P. *Biopolymers* **2002**, *65*, 395–407.

on LB media and incubating at 37 °C O/N. Initial viable cell densities for all experiments were ~10^5 CFU/mL.

2.2. Nanoparticle Synthesis and Characterization. ZnO NPs (13 nm) were synthesized in diethylene glycol (DEG) via the forced hydrolysis of zinc acetate as reported previously.[2] The average particle diameter was confirmed to be 13.7 ± 2.0 nm by transmission electron microscopy (TEM) and X-ray diffraction, with some observed particle agglomerates ranging in diameter from 200 to 400 nm. TEM coupled with energy-dispersive spectroscopy (EDS) was employed to visualize the association of the 13 nm ZnO NPs and the cell surface of the PAO1 strains (data not shown).

2.3. NP Exposure Experiments. To determine the ZnO NP MIC, each strain was incubated in 100 μL of LB amended with NPs in the 1−4.25 mM range in black-walled 96-well plates (Corning; Corning, NY). Cytotoxic effects of NP exposure were determined by enumerating viable CFU/mL and a measure of metabolic activity (i.e., Alamar blue detection) after incubation. Alamar blue is a cell-permeable redox-sensitive dye that turns from a nonfluorescent blue color to a highly fluorescent pink color (excitation/emission 530/590 nm, respectively) upon reduction by cellular metabolic activity[38] and has been used extensively for assessing the metabolic activity of cells in culture. All experimental treatments were amended with 10% Alamar blue to enable the fluorescent detection of metabolic activity. Fluorescent detection of the reduced Alamar blue signal was performed in a Synergy HT fluorescent microplate reader (BioTek, Winooski, VT). Ninety-six-well plates were sealed with optical adhesive covers (Applied Biosystems, Foster City, CA) to prevent evaporation, incubated at 37 °C, and read at 0, 24, 48, and 72 h or until no additional change in the Alamar blue signal was detected. For all treatment levels and strains, the Alamar blue signals did not change after 72 h of incubation; therefore, only the 72 h time-point data are analyzed here. To confirm if the Alamar blue signals were indicative of cell proliferation, inhibition, or death, samples of each experimental treatment were diluted, as necessary, in sterile LB after 72 h of exposure to NPs, plated on NP-free LB plates, incubated at 37 °C O/N; then CFU/mL values were determined. All experiments were performed in quadruplicate ($n = 4$).

2.4. Effect of Coincubation with CaCl$_2$ on ZnO NP Toxicity. To further assess the role of electrostatic interactions in controlling the antimicrobial activity of ZnO NPs against *P. aeruginosa*, we exposed the PAO1 strains to ZnO NP concentrations above and below their respective MICs in the presence of a range of divalent cation (Ca^{2+}) levels (0, 3, 5, and 7.5 mM CaCl$_2$). To assess the influence of CaCl$_2$, experimental treatments were amended with 10% Alamar blue to enable the fluorescent detection of metabolic activity. Fluorescent detection of the reduced Alamar blue signal was performed as described above. CaCl$_2$ is a nontoxic compatible solute for many bacteria. However, to confirm the noninhibitory nature of CaCl$_2$, ZnO NP-free control treatments were established for all CaCl$_2$ treatment levels employed here. No effect of CaCl$_2$ exposure on PAO1 growth was observed (data not shown). In addition, sterile controls for CaCl$_2$ with and without ZnO NP treatments were performed to correct for any background reduction of the Alamar blue dye. Fluorescence observed in the sterile treatments was subtracted from the nonsterile treatment signals prior to analysis. All experiments were performed in quadruplicate ($n = 4$) in black-walled 96-well plates as above. To confirm that the Alamar blue signals were indicative of cell proliferation, inhibition, or death, after

48 h of incubation, samples of each experimental treatment were diluted, as necessary, in sterile 0.9% NaCl and plated onto NP-free LB plates and then incubated at 37 °C O/N to determined CFU/mL.

2.5. Statistical Analyses. Microbial viability data (i.e., CFU/ml and Alamar blue fluorescence) were analyzed by analysis of variance (ANOVA). All statistical tests were performed using SPSS v11.0.4 software (SPSS Inc., Chicago, IL), and p values of ≤0.05 were considered to be indicative of statistically significant interactions (i.e., the observed differences in strain responses to the experimental treatments had at least a 95% probability of not being due to chance alone).

3. Theory and Modeling

3.1. Model System. We built on a recent minimum model[34] to establish whether electrostatics and saccharide−saccharide bonding play important roles in determining the dependence of the relative MIC of ZnO NPs on bacterial strain. In modeling the system, we must consider (a) the outer membrane of *P. aeruginosa*, (b) the aqueous solution with which the outer membrane is in contact, with or without ions, and (c) the charged ZnO NP. The characteristic length and timescales must be able to model a system involving spherical NPs with mean radius of ~6.5 nm and ionic concentrations corresponding to Debye screening lengths of $\kappa^{-1} \approx 1$ to 2 nm. Accordingly, if we use computer simulation, then we must model an area of an outer membrane that is >20 nm on each side. We use periodic boundary conditions (PBCs) in directions parallel to the surface of the outer membrane but not perpendicular to that surface (the z axis), which is the direction with respect to the "bulk" aqueous solution.

Figure 1 shows the model system comprising (a) a hydrophobic dielectric layer, (c/b) LPS molecules with/without O side chains, (d) the aqueous solution with Na$^+$, Cl$^-$, and Ca^{2+} ions, and (e) a dielectric NP. In our model, the LPS molecules comprised two spheres representing the hydrocarbon chains anchoring the LPS in the membrane and a core made up of six sugar groups with negative charges and six uncharged sugar groups.[29] The hydrocarbon chain region plays no role other than (i) constraining the polysaccharides to lie in the water region, (ii) keeping their bases at the oil/water interface a certain distance apart that is characteristic of such a membrane in its fluid phase,[29] and (iii) providing a dielectric slab that can be polarized by charges in the aqueous solution. Although we could have represented the hydrocarbon chains by simply a disk on the surface of the membrane or even a soft cylinder, we found that it was simpler to represent them by spheres in order to facilitate diffusion in the plane of the membrane. We refer to such spheres as anchoring spheres. Sugar groups were represented by spheres, and the polymers were semiflexible.[30] Unit vectors $\hat{x}$ and $\hat{y}$ were in the $x−y$ plane (the plane of the membrane), and $\hat{z}$ was along the z axis, perpendicular to the membrane (Figure 1).

All charges were integers ($+1, −1, +2$) in proton charge units of $e = 1.602 \times 10^{-19}$ C. Ions in solution were spherical, and all sugar and ion spheres had the appropriate charge located at their centers. To simplify the simulation, charges on the NP sphere were located on 100 uniformly distributed locations at a depth of 0.10 nm inside the geometrical surface of the NP.

3.2. Electrostatic Interactions. The aqueous solution ($z > 0$) and the hydrocarbon-chain region ($z < 0$) were represented as two dielectric continuums with relative permittivities of $\varepsilon_w = 81$ and $\varepsilon_{hc} = 5$, respectively,[31] and we represented monovalent ion screening in the aqueous solution by linearized

(38) Page, B.; Page, M.; Noel, C. *Int. J. Oncol.* **1993**, *3*, 473−476.

Poisson−Boltzmann theory.[29,38−40] Although the representation of monovalent ions via Poisson−Boltzmann theory, which is a mean field theory, can be justified, the same cannot be said of multivalent ions, specifically, Ca^{2+} ions. Ca^{2+} ions can form dynamic bridges with pairs of negatively charged moieties and thus take part in highly correlated three-body interactions that are generally inadequately described by mean field theory. Accordingly, all Ca^{2+} ions and their associated Cl^- ions were represented by explicit ion spheres. We calculated the electric potential at $\vec{R} = x\hat{x} + y\hat{y} + z\hat{z}$ due to an electric charge Q at $\vec{R}_0 = x_0\hat{x} + y_0\hat{y} + z_0\hat{z}$ in the aqueous solution. Netz[35,36] derived expressions for the electrical potential at $\vec{R}$ (eqs 14 and 15 in ref 36.). Defining $\eta = \varepsilon_{hp}/\varepsilon_w$ and $\chi = (1 - \eta)/(1 - \eta)$, then, because $\varepsilon_{hp} \ll \varepsilon_w$, the electrical potential at $\vec{R}$ becomes

$$V(Q, \vec{R}_0, \vec{R}) = \left(\frac{1}{4\pi\varepsilon_w\varepsilon_0}\right)\sum_j Q_j f(|\vec{R}_j|),$$

$$f(|\vec{R}_j|) = \frac{e^{-\kappa|\vec{R}_j|}}{|\vec{R}_j|} \qquad (1)$$

where the sum is over $j = 1$ to 2, $\vec{R}_1 = \vec{R} - \vec{R}_0$, $\vec{R}_2 = \vec{R} - \vec{R}_0 + 2z_0\hat{z}$, $Q_1 = Q$, $Q_2 = \chi Q$, κ^{-1} is the Debye screening length, and ε_0 is the permittivity of free space. $V(Q, \vec{R}_0, \vec{R})$ goes to the correct limiting values as $\varepsilon_{hp} \to 0$ and as $\kappa \to 0$.

3.3. Zeta Potential and Electric Charge. The surface potential, $V(q, R_0)$, associated with a spherically symmetric NP is

$$V(q, R_0) = \frac{q/(1 + \kappa R_0^+)}{4\pi\varepsilon_0\varepsilon_w R_0^+} \qquad (2)$$

where $q \equiv \pm eQ$ ($Q = 0, 1, 2,...$) is the total charge, bulk, and surface (including the Stern layer) of the NP of radius R_0 and $R_0^+ = R_0 + \delta$ with $\delta \approx 0$. We calculate the surface potential a small distance into the water in order to include the tightly bound Stern layer. Zeta potential measurements were performed to help parametrize model characteristics associated with NP surface charge. Zeta potentials of powdered samples of ZnO NPs (average diameter ∼13 nm) suspended in nanopure water were measured with a Malvern Zetasizer NanoZS. The temperature was equilibrated to 25 °C, and the pH was adjusted to ∼7.5 using 1.0 N HCl and 1.0 N NaOH prior to collecting the data. At least eight data collections per run were performed on four independently synthesized ZnO samples, yielding an average zeta potential of 38.7 ± 1.8 mV. At this pH and ion concentration, $\kappa \approx 0.03$ nm^{-1}. When $R_0 = 6.5$ nm, we find that $V(eQ, 6.5) = 2.29Q$ mV so that, with an average zeta potential of 38.7 mV, $Q \approx 17 \pm 0.8$. We chose to model $Q = 10$ and 100 to study limiting cases.

3.4. Bonding. A physical bond of energy E_B may form between a pair of sugar spheres that are a center-to-center distance R apart if $R \leq R_B$. We chose $R_B = 0.5$ nm, a distance typical of hydrogen bonding. For the bond energy, we chose $E_B = 0.4 \times 10^{-20}$ J, a value slightly lower than $k_B T$ at 30 °C and typical of hydrogen bonding energies.

3.5. System Parameters. Our simulation membrane plane possessed dimensions of 32.0×27.8 nm^2, which accommodated 400 LPS molecules. The z dimension of the simulation volume ranged over $0 \leq z \leq 30.0$ nm. The "bulk" was taken to be the volume ranging over $20.0 \leq z \leq 30.0$ nm. For computational simplicity, the Stern layer charge was equally distributed over 100 sites lying 0.1 nm below the geometrical surface of the NP

(above) and ranged in magnitude from $Q = 10$ (0.1e per site) to $Q = 200$ (2.0e per site). The radius of each sugar sphere was $R_{sugar} = 0.15$ nm,[29] and the equilibrium stretchable bond length was $L_0 = 0.52$ nm.[39−41] The relative angle between adjacent saccharide−saccharide bonds was $30 \pm 10°$.[30] The hydrocarbon chain region of an LPS, represented by the two spheres that serve to anchor and move the polysaccharides in the plane of the membrane, each had a radius of $R_{anchor} = 0.70$ nm (Figure 1). The sphere closer to the water region possessed an equilibrium position of $z_0 = -0.40$ nm and could move along the z axis by ±0.15 nm from equilibrium. The second sphere was connected to the first sphere via a center-to-center bond that could stretch from 1.0 to 1.5 nm. These "anchoring spheres" (above) could rotate around their centers and so reorient the polysaccharide chains, but no sugar moiety or ion could move into the region of $z < 0$. Hydrated ions were represented by spheres of radius $R_I = 0.18$ nm, with charges located at their centers. We chose $\kappa = 0.5$ nm^{-1} (ionic strength ∼25 mM) and added monovalent ions until we had acquired an average of ∼304 Na^+ and Cl^- ions in equilibrium in the bulk so that those "explicit" monovalent ions contributed an effective Debye screening length of $\wr_2$ corresponding to $\kappa_2 = 0.866$ nm^{-1} (ionic strength ∼75 mM). This procedure resulted in an effective total bulk inverse Debye length of $\kappa_t = (\kappa^2 + \kappa_2^2)^{1/2} \approx 1.0$ nm^{-1}. We restricted the maximum distance over which we took into account the electrostatic interaction to 4.0 nm. We added sufficient Ca^{2+} ions to ensure that the core region was saturated with divalent cations in order to mimic conditions at the surface of a bacterium. We then added Cl^- ions so that charge neutrality in the bulk was maintained. We considered three cases: (a) zero additional Ca^{2+} ions (Ca-free buffer), (b) a "low" concentration of Ca^{2+} ions in the bulk (∼10 mM), and (c) a "high" concentration in the bulk (∼40 mM). The system was equilibrated at $T = 27$ °C for 10^5 Monte Carlo steps, and the properties of the system were measured for $\geq 10^5$ steps.

Unit vectors $\hat{x}$ and $\hat{y}$ were in the $x-y$ plane (the plane of the membrane), and $\hat{z}$ was along the z axis (Figure 1). We used Monte Carlo (MC) simulation methods[42−44] with periodic boundary conditions along the x and y axes. At each MC step, we attempted to change the position of all moieties consistent with two requirements: no two moieties should overlap, and no water-soluble moiety was permitted to enter the region $z < 0$. We computed the energy of the NP as a function of its position along the z axis by fixing its center at one position, carrying out the MC procedure to bring the surroundings of the NP to thermal equilibrium, and then continuing the MC procedure to obtain thermal averages with standard deviations for the energy of the NP.

4. Results and Discussion

4.1. Model-Based Prediction of Relative ZnO MIC. Figure 2 shows the average energy, $E(S, z)$, of an NP with its center at z for strain, S, of *P. aeruginosa* for NP charges $Q = 10$ and 100. The range of $z \geq 7.0$ nm was chosen because the radius of the NP is 6.5 nm and it was not possible to place the NP closer to the membrane surface to calculate the energy.

4.1.1. Q = 10. As the NP approaches the cell surface, the energy is repulsive because of the presence of Ca^{2+} ions in the core for all strains, except in the case of a rough mutant

(39) Carmesin, I.; Kremer, K. *Macromolecules* **2002**, *21*, 2819–2823.
(40) Stevens, M. J.; Kremer, K. *Phys. Rev. Lett.* **1993**, *71*, 2228.

(41) Chen, H.; Zajac, R.; Chakrabarti, A. *J. Chem. Phys.* **1996**, *104*, 1579–88.
(42) Metropolis, N.; Rosenbluth, A. W.; Rosenbluth, M. N.; Teller, A. H.; Teller, E. *J. Chem. Phys.* **1953**, *21*, 1087–1092.
(43) Lai, P.-Y.; Binder, K. *J. Chem. Phys.* **1992**, *97*, 586–595.
(44) Binder, K.; Heermann, D. W. *Monte Carlo Simulation in Statistical Physics: An Introduction*; Springer: Berlin, 1988.

A⁻B⁻ bacterium when the excess Ca²⁺ concentration is low or high (Figure 2A, yellow curves). In that case, the center of the NP can get within ∼7.5 nm of the surface. In general, as the bulk Ca²⁺ ion concentration is increased, the energies become more repulsive. With the exception of the A⁻B⁻ bacterium, all energies are monotonically increasing as the NP approaches the bacterial surface. From this, we would conclude that the NP MICs should follow the inequalities A⁻B⁻ < A⁺B⁻ ≈ A⁻B⁺ ≈ A⁺B⁺.

4.1.2. Q = 100. At a net NP charge of 100, the data fall into three sets: (a) A⁻B⁺, (b) A⁻B⁻ and A⁺B⁻, and (c) A⁺B⁺ (Figure 2B,D). For the lower-energy set (a), A⁻B⁺, there is a broad minimum at around 8.5 nm that is most pronounced when there is zero excess Ca²⁺ and that broadens and moves away from the membrane as divalent ions are added. One would expect an NP to be trapped in it when there is zero excess Ca²⁺ (i.e., the NP should be held close to the cell surface when Ca²⁺ levels are low). Overall, the energy becomes less negative as divalent ions are added. The higher-energy set (b), A⁻B⁻ and A⁺B⁻, exhibits a long-range repulsion for the NP, with very weak energy minima at around 8 to 9 nm. The repulsive barrier that rises as the distance from the membrane decreases is likely due to the Ca²⁺ layer in the

core. Set (c), A⁺B⁺, is also a higher-energy set. In the absence of excess Ca²⁺ ions, this case exhibits a shallow energy minimum near 8 nm that moves to 8.5 nm and becomes deeper as divalent ions are introduced. However, the energy is near zero, and as more divalent ions are added (∼40 mM), the potential becomes steeply repulsive near the membrane surface. Upon the basis of this, we predict that A⁻B⁺ is most vulnerable to attack by NPs but that A⁺B⁺ will be most resistant in the presence of divalent ions. The fact that an energy minimum exists for A⁻B⁺ is not necessarily protection for the bacterium: the NP being held within 1 nm of the surface would be localized there while it inhibited the bacterium.

On the basis of these results, the sequences of MICs were predicted to be approximately A⁻B⁺ < A⁺B⁺, A⁻B⁻, A⁺B⁻ (no excess Ca²⁺) and A⁻B⁺ < A⁺B⁻ < A⁻B⁻ < A⁺B⁺ (excess Ca²⁺). In the Conclusions section, we discuss whether the experimental no-excess Ca²⁺ case does indeed correspond to no excess Ca²⁺.

4.2. Experimental Assessment of Model Predictions. To test the predictions of the electrostatic modeling, all four strains of PAO1 were exposed to different concentrations of ZnO NPs, with and without excess Ca²⁺ present in the growth media. Specifically, we performed experiments to address the following questions: Are more highly charged cells more susceptible to ZnO NP toxicity? Can differences in ZnO NP resistance among strains be explained by modeling electrostatic interactions between individual 13 nm ZnO NPs and the LPS layer of the outer membrane of PAO1?

Significant differences in MICs were detected among strains as measured by both Alamar blue dye conversion and CFU/mL assessments (F_{alamar} = 2.88, $P < 0.001$) (Figure 3). The A⁻B⁺ strain with the most highly charged LPS layer was the most susceptible to the ZnO NP treatment, demonstrating the lowest MIC (3.25 mM ZnO, as determined by Alamar blue reduction). This is in agreement with the predicted responses for an NP with a net charge of 100. The wild-type strain (A⁺B⁺) with a mixture of charged and uncharged oligosaccharides in its LPS was the most resistant to ZnO NPs, with MIC = 4.25 mM. The two strains with only uncharged oligosaccharides or no O side chains (A⁻B⁻ and A⁺B⁻, respectively) had moderate and approximately equal levels of resistance to ZnO NPs with MICs = 3.5 and 3.75 mM, respectively. The intermediate responses of the A⁺B⁻ and A⁻B⁻ strains were expected, on the basis of the energy predictions for an NP with its center in the range of 7−10 nm from the cell surface (Figure 3). However, what was not expected was the relative
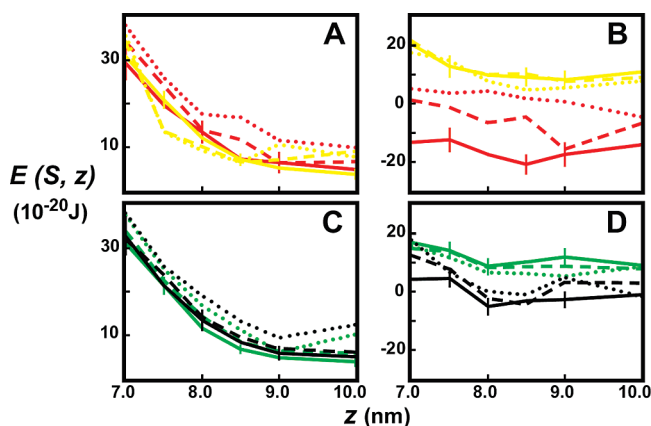
Figure 2. Average energies, $E(S, z)$, of an NP for the strain, S, of *P. aeruginosa*, modeled under standard incubation conditions as a function of the position, z, of the center of an NP carrying total charges of $Q = 10$ (A, C) and 100 (B, D). (A, B) A⁻B⁺ (red) and A⁻B⁻ (yellow). (C, D) A⁺B⁺ (black) and A⁺B⁻ (green). There is no excess CaCl₂ in the bulk (solid lines), ∼10 mM excess CaCl₂ in the bulk (dashed lines), and ∼40 mM excess CaCl₂ in the bulk (dotted lines). At 37 °C, the magnitude of the thermal energy is $3k_BT/2 = 0.642$. Typical standard deviations are shown.
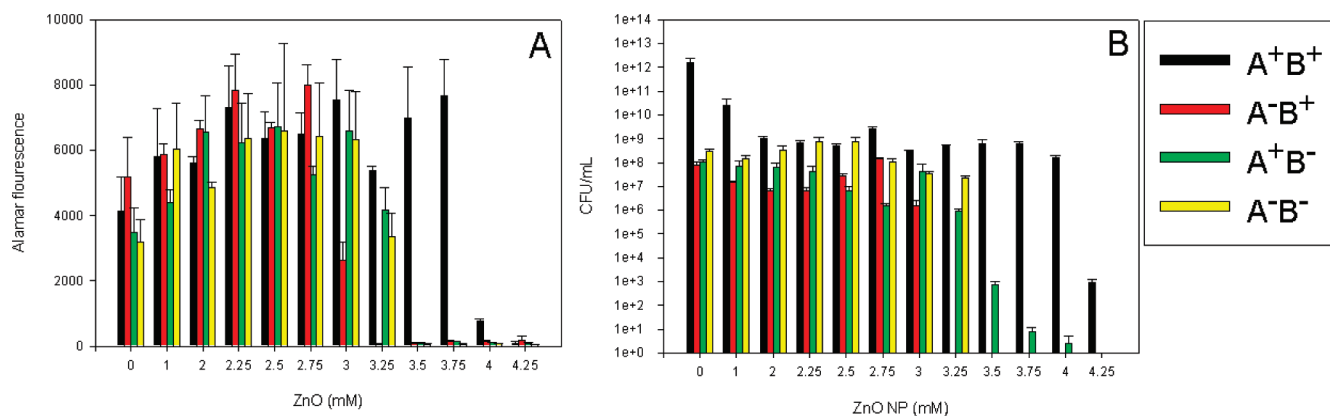
Figure 3. Relative sensitivity of *P. aeruginosa* PAO1 strains to 13 nm ZnO nanoparticles measured after 72 h of incubation. (A) Influence of ZnO NPs on cellular metabolism as assessed by Alamar blue reduction. (B) Effects of ZnO NP exposure on cell viability, expressed as CFU/mL. Alamar fluorescence is a relative measure of the metabolic activity of the PAO1 cells present in each experimental treatment.

resistance of A^+B^+ to ZnO NP when there is no excess Ca^{2+}. This apparent discrepancy might be understood when one considers the effect of excess Ca^{2+} concentrations in the bulk. It is likely that the nutrient solution itself contains divalent cations and that what was assumed to be a zero-excess Ca^{2+} case was in fact one containing excess Ca^{2+} in the bulk solution. Indeed, the growth medium employed here (LB) typically contains approximately 80−200 μM unbound Ca^{2+},[45] suggesting that our experiments in which we did not amend with $CaCl_2$ likely contained a small excess of Ca^{2+}.

If ZnO NPs carry a net positive charge and if the electrostatic attraction between the NPs and PAO1 LPS controls, in part, the toxicity of ZnO NPs, then the coincubation of cells with NPs and a positively charged compatible solute, such as calcium chloride ($CaCl_2$), should reduce the effectiveness of ZnO NPs as a cytotoxic or antibacterial substance. Indeed, the electrostatic modeling predicts a positive shift in energy, implying a greater repulsion (or a reduced attraction) between the cell surface and the NPs when elevated levels of calcium ions (Ca^{2+}) are present (Figure 2).

Calcium is a common cationic solute present in the LPS layer and cytoplasm of gram-negative organisms.[46] The positive charge of Ca^{2+} should help to repel a positively charged NP from the cell and prevent binding to the negatively charged LPS O side chains on the cell surface, thereby alleviating the toxicity of ZnO NPs. This argument does not take into account Ca^{2+} entropy losses; however, we have observed[29] that model Ca^{2+} ions hop between energy minima and so do not lose all of their entropy in binding near the surface. The modeling of this interaction supports this hypothesis and suggests that the relative sensitivities of the four PAO1 strains will remain the same but the extent of NP-induced inhibition will be reduced relative to what is observed in the absence of elevated Ca^{2+}, as reflected by the movement of the energy of interaction toward more neutral values (Figure 2). Furthermore, the effect of Ca^{2+} on ZnO NP toxicity should be concentration-dependent such that by increasing the Ca^{2+} concentration one could incrementally decrease the cytotoxicity of ZnO NPs.

To test these predictions, we exposed all four strains of PAO1 to ZnO NPs above and below their respective MICs in the presence of 0, 3, 5, and 7.5 mM $CaCl_2$ as described above for the Alamar-based detection of ZnO NP toxicity. ZnO NP-free controls were established for all $CaCl_2$ treatment levels, and no effect of $CaCl_2$ exposure on PAO1 growth was observed (data not shown). The ability of $CaCl_2$ to alleviate ZnO NP toxicity among the different strains differed as indicated by a statistically significant interaction between the strain type and the level of $CaCl_2$ applied in the presence of ZnO NP ($F_{PAO1strainxCaCl_2}$ = 3.339, p = 0.001). The effect of Ca^{2+} amendment was most pronounced in the A^-B^+ and A^+B^+ strains (Figure 4). At ZnO concentrations below the MIC for A^-B^+ (i.e., <3.25 mM), Ca^{2+} amendment had no significant effect on metabolic activity (data not shown). However, in the presence of ZnO at or above the MIC (i.e., ≥ 3.25 mM), amendment with Ca^{2+} at 3 mM resulted in the full recovery of growth equivalent to no NP controls. Ca^{2+} concentrations above 3 mM resulted in no further increase in metabolic activity, indicating that the threshold for full recovery from ZnO NP toxicity is below the lowest concentration of Ca^{2+} tested (i.e., <3 mM Ca^{2+}) for alleviating ZnO NP toxicity at concentrations of up to 3.75 mM. These results suggest that the coincubation of
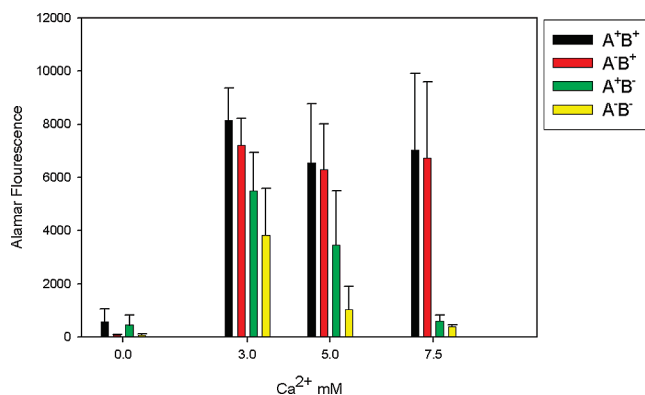

Figure 4. Effect of $CaCl_2$ addition on ZnO NP toxicity with respect to *P. aeruginosa* PAO1 strains at their respective MICs. Influence of a 72 h co-incubation of ZnO NPs and $CaCl_2$ on cellular metabolism, as assessed by Alamar blue reduction.

A^-B^+ with positively charged ZnO NPs and a compatible positively charged ion reduces the toxicity of ZnO NPs. Similar results were observed for the wild-type PAO1 strain (A^+B^+) (Figure 4). Although this strain has a higher inherent tolerance to ZnO NPs, the presence of a positively charged compatible ion provided relief from ZnO toxicity. The binding of Ca^{2+} to the charged O side chains in both of these strains[34] may lower the net surface charge of these cells, thereby reducing the electrostatic attraction between the NPs and the cell surface. The A^+B^- and A^-B^- strains (i.e., those carrying no charged O side chains or no charged or uncharged O side chains) were predicted to demonstrate a less dramatic response to Ca^{2+} amendment because of their predominantly uncharged nature. Under elevated Ca^{2+} concentrations, the calculated energies of interaction for these strains become less positive, although the change in energies is smaller in magnitude than that for A^-B^+ and A^+B^+ (Figure 2). Therefore, the NPs may be repelled less strongly from the surfaces of the A^+B^- and A^-B^- cells, making the ZnO NPs a more effective inhibitor. Indeed, we observed a significant decrease in metabolism for these two strains as we increased the Ca^{2+} concentration under constant ZnO exposure (Figure 4). However, factors other than electrostatic attraction may play a role in modulating NP cytoxicity. For example, growth temperature and salt concentration can affect the expression level and length of the A- and B-band O side chains.[32,47] A reduction in O side chain number and length could explain the increased toxicity of the NP treatment at $CaCl_2$ concentrations above 3 mM for the B^- strains if the LPS modification allowed the NP to be held closer to the cell surface, thereby increasing the NP toxicity.

When combined, our data suggest that the electrostatic attraction between the cell and the NP surfaces controls part of the NP cytotoxicity in our system and that the electrostatic control is context-dependent (i.e., dependent upon whether compatible solutes, with charge similar to that for the NPs, are present and at what concentration). Additional study is required to determine what specific LPS expression modulations are induced by NP exposure and how this might affect NP cytotoxicity.

5. Conclusions

We calculated the energies of an NP with a diameter of 13 nm as a function of the distance, z, from the outer surface of the cell of

(45) Boehm, D. F.; Welch, R. A.; Snyder, I. S. *Infect. Immun.* **1990**, *58*, 1951–1958.

(46) Poole, R. K. *Advances in Microbial Physiology*; Academic Press: 2009; Vol. 55, p iii.

(47) McGroarty, E. J.; Rivera, M. *Infect. Immun.* **1990**, *58*, 1030–1037.

four *P. aeruginosa* strains (A^-B^-, A^+B^-, A^-B^+, and A^+B^+) as functions of $CaCl_2$ in the system. From the results of measurements of the zeta potential, we argued that the NP possessed approximately 17 ± 0.8 proton charges. We carried out simulations of an NP possessing a total of 10 and 100 such charges uniformly distributed over its surface, and we considered three concentrations of excess $CaCl_2$: 0, ~10, and ~40 mM. The system was initially equilibrated with excess $CaCl_2$, and after the Ca^{2+} ions had migrated into the core region of the LPS, excess ions in the bulk, sufficiently far from the membrane surface, were removed. Excess ions were restored by adding ions to the bulk until the desired bulk concentration had been achieved. Our results predict that the MICs of this system should obey the following inequalities:

(1) For $Q = 10$, the MICs for the four strains should follow $A^-B^- < A^+B^- \approx A^-B^+ \approx A^+B^+$. The effect of increasing the number of Ca^{2+} ions was to increase the energy barrier and repel the NP from the membrane surface. In this case, the charge on the NP is not sufficiently large to lead to an attraction that could trap the NP sufficiently close to the membrane surface to inhibit the bacterium.

(2) For $Q = 100$, the case closest to that investigated here experimentally, the MICs should follow $A^-B^+ < A^+B^+$, A^-B^-, A^+B^- for zero excess Ca^{2+} ion concentration. For excess Ca^{2+}, the MICs should follow the inequalities $A^-B^+ < A^+B^- < A^-B^-$, A^+B^+. The most striking result is that the A^-B^+ bacterium is by far the most susceptible to attack by ZnO NPs. The reason for this can be seen in an inspection of instantaneous conformations of the surface: the NP is trapped by the negatively charged O side chains that are attracted to the positive charges on the NP surface. The O side chains form a "forest" around the NP. The location of the minimum in the energy corresponds to the maximum attractive interaction where the O side chains can engulf the NP. Although the same effect can take place for the A^+B^+ bacterium, it is inhibited by the fewer number of negatively charged O side chains and by the presence of the uncharged O side chains that serve to repel the NP from the surface. Clearly this effect must depend upon the characteristic lengths of the O side chains. However, this does not change our results: A^-B^+ will be the most susceptible to attack by sufficiently positively charged NPs. We have suggested that the experimental case in which we have not explicitly added excess Ca^{2+} to the system does, however, fall under an excess Ca^{2+} model because the nutrient solution is likely to contain divalent cations.

The importance of electrostatic attraction between bacterial cells and surfaces has been known for some time and is usually discussed in the context of biofilm formation.[48−51] It appears that for metal oxide NPs the electrostatic interaction is also important for the initial attraction and eventual cytotoxicity.[52] For example, NP attachment to bacterial surfaces appears to be essential for cytotoxicity[53] and altering the surface charges of either a metallic substrate or the bacteria can greatly influence bacteria−metal adhesion forces.[54] Furthermore, the inclusion of dispersants

capable of disrupting non-charge-based interactions, such as polyethylene glycol and polyvinylpyrolidone, has a small effect on the attraction of NPs and model bacterial surfaces, thereby suggesting that electrostatics plays a stronger role in attraction than do hydrophobic interactions.[55] Our findings suggest that it is likely that the association of metal oxide NPs to a bacterial cell is mediated by electrostatic attraction and that the strength of this association is dependent on the conditions under which the NP and cells are exposed. Although it has been demonstrated that ZnO NP may be able to enter bacterial cells,[7,8] our data and that of others suggest that electrostatic attraction at the bacterial surface is central to much of the antibacterial activity. For example, Liu et al.6 used Raman spectroscopy to demonstrate that exposure to ZnO NPs damaged the membrane of *E. coli* O157:H7 but not the intracellular macromolecular structures, implying that the mode of action occurs at the surface of the cell.[6]

Given that ZnO NPs appear to have the potential to produce reactive oxygen species (ROS),[26−28] localization of the particles close to the cell surface could lead to ROS accumulation and subsequent cellular damage. ROS generation could be achieved via particle dissolution and subsequent Zn-dependent ROS formation catalyzed by the soluble NP components or by direct NP-dependent ROS formation, as demonstrated elsewhere.[28] Although certain synthesis methods for generating ZnO NPs can allow the NP to dissolve,[9] the availability of zinc ions via ZnO NP dissolution does not explain the observed toxicity. The incubation of all four PAO1 strains with $ZnCl_2$ at concentrations well above the ZnO NP MICs resulted in no inhibition of growth (data not shown). NP dissolution in combination with membrane disruption could also result in ROS formation if dissolution produced the oxygen necessary for the formation and accumulation of a superoxide anion close to the cell surface. A superoxide can be formed in solution by combining O_2 with free electrons released or "leaked" from the bacterial electron-transport chain by allowing contact between O_2 and reduced quinones.[56] If localization of the NP near the bacterial surface results in membrane disruption, as suggested by others,[6,8,55] the subsequent release of reduced components of the electron-transport chain could result in additional oxidative cellular damage at the cell surface. Regardless of the generation mechanism, ROS molecules that formed near the cell surface would have a greater inhibitory or damaging effect if the ROS generation source (i.e., the NP) was held close to the cell surface.

Collectively, our data indicate that cells with charged outer-membrane surfaces are most susceptible to ZnO NP treatment and that the presence of similarly charged compatible solutes can ameliorate the cytotoxic effect of ZnO NPs. It follows that modifications to NPs, physiological responses of target cells, or modification of media constituents that affect NP or cell surface charge should alter the cytotoxic efficacy of metal oxide NPs. We propose that the modification of NP surface charge may prove to be a fruitful approach to modulating the cytotoxic properties of metal oxide NPs.

(48) Chen, X.; Stewart, P. S. *Appl. Microbiol. Biotechnol.* **2002**, *59*, 718–720.

(49) Stoodley, P.; deBeer, D.; Lappin-Scott, H. M. *Antimicrob. Agents Chemother.* **1997**, *41*, 1876–1879.

(50) Hong, L.; Herbert, H. P. F. *Biotechnol. Bioeng.* **2002**, *80*, 806–811.

(51) Ghannoum, M. A.; O'Toole, G. A. *Microbial Biofilms*; ASM Press: Herndon, VA, 2004; Vol. *1*, p 476.

(52) Stoimenov, P. K.; Klinger, R. L.; Marchin, G. L.; Klabunde, K. J. *Langmuir* **2002**, *18*, 6679–6686.

(53) Jiang, W.; Mashayekhi, H.; Xing, B. *Environ. Pollut.* **2009**, *157*, 1619–1625.

(54) Sheng, X.; Ting, Y. P.; Pehkonen, S. O. *J. Colloid Interface Sci.* **2008**, *321*, 256–264.

(55) Zhang, L.; Jiang, Y.; Ding, Y.; Povey, M.; York, D. *J. Nanopart. Res.* **2007**, *9*, 479–489.

(56) Fridovich, I. *Oxygen Radicals, Hydrogen Peroxide, and Oxygen Toxicity*; Academic Press: New York, 1976; Vol. *1*, pp 239−277.